CO-DIFFUSED BACK-CONTACT BACK-JUNCTION SILICON SOLAR CELLS

Roman Keding[1,2], David Stüwe[1], Mathias Kamp[1], Christian Reichel[1], Andreas Wolf[1], Robert Woehl[1*], Dietmar Borchert[1], Holger Reinecke[3], and Daniel Biro[1]

[1]Fraunhofer Institute for Solar Energy Systems, Heidenhoferstraße 2, D-79110 Freiburg, Germany
[2]Freiburg Material Research Center, University of Freiburg, Stefan-Maier-Straße 21, D-79104 Freiburg, Germany
[3]Institute for Microsystems Engineering, University of Freiburg, Georges-Köhler-Allee 103, D-79110 Freiburg, Germany
[*]Now with Total New Energies, 5858 Horton Street, Emeryville, CA 94608, USA

ABSTRACT: In this work first generation Back-Contact Back-Junction (BC-BJ) silicon solar cells with cell efficiencies well above 20 % were fabricated. The process sequence is industrially feasible, requires not more than two high-temperature steps (co-diffusion and drive-in), and implements only industrially available pattering technologies. The silicon-doping is performed from pre-patterned solid diffusion sources, which allow for the precise adjustment of phosphorus and boron doping-levels. Based on the investigated process technologies BC-BJ solar cells without gap between adjacent n^+- and p^+-doped areas are processed. On the one hand, a strong reduction of the process effort is possible by omitting the gap regions. On the other hand, parasitic tunneling currents through the narrow space charge region may occur. Hence, deep doped areas were realized to avoid tunneling currents in gap-free BC-BJ cells. The paper finishes with a detailed characterization of the manufactured cells including important cell measurements like IV and $Suns V_{OC}$.

Keywords: devices, diffusion, PECVD

1 INTRODUCTION

The main difference between BC-BJ and standard solar cells is, that the electrical contacting of silicon and thus the extraction of excess carriers is carried out on the rear side of the cell. Hence, shading losses due to a metal grid on the front side are completely avoided, resulting in an increased photo current and efficiency of the cell [1]. An advanced module assembly of BC-BJ solar cells is reported as well, since the cell to cell wiring by cell connectors is only performed on the rear side [2].

But, there are also some challenges. Firstly, a highly efficient BC-BJ solar cell usually exhibits three different doped areas: The so-called front surface field (FSF), the back surface field (BSF), and the emitter. Hence, several diffusion steps with high process temperatures have to be carried out, leading to an increase in process costs. Secondly, for an efficient collection of excess carriers, locally doped areas have to be integrated on the rear side. The successful integration of locally doped areas in BC-BJ cells depends strongly on resolution and accuracy of the used patterning technologies. Unfortunately, the implementation of patterning technologies in the process sequence leads to a further increase in process effort. Thirdly, since excess carriers are generated on the front side and collected at the *pn*-junction on the rear side, the solar cell performance depends strongly on the front surface passivation, bulk carrier life time, and especially the wafer thickness. In conclusion, the higher efficiency potential of BC-BJ solar cells compared to standard silicon solar cells can only be fully exploited, if the additional process effort and costs of this advanced cell type are kept as low as possible.

This work presents BC-BJ solar cells manufactured in an industrially feasible manner [3]. One single high temperature treatment, the so called co-diffusion, forms all necessary doped areas. Therefore pre-patterned solid diffusion sources are used. A highly precise inkjet process enables patterning of both, solid diffusion sources and metallization, allowing for minimal feature sizes below 50 µm. Aiming at even further reducing the process effort, BC-BJ solar cells are manufactured without gap between adjacent n^+- and p^+-doped areas on the rear side of the cell. Compared to cells with gap, one patterning step can be omitted in this case. To prevent tunneling recombination currents in gap free BC-BJ solar cells, deeply diffused doped areas were integrated. The presented BC-BJ process flow solely relies on processing steps without mechanical contact to the cell. By aiming at further reduction of the overall material costs, also ultra-thin wafers could be introduced as base material.

The second chapter of this work focuses on the BC-BJ solar cell design and the corresponding process chain used within this work. A more detailed view on the co-diffusion process and the influence of the drive-in process on co-diffused doped areas is given as well. In the third chapter, the performance of the manufactured solar cells is discussed. Therefore, co-diffused cells with and without drive-in are compared. The influence of the deposition processes on the cell performance is investigated, by comparing cell results of cells diffused from two different solid boron diffusion sources. Finally, in the fourth chapter, a plating step is carried out to improve the cell performance and to characterize external series resistance losses.

2 SOLAR CELL PROCESS TECHNOLOGY

2.1 Process chain

The process chain of the BC-BJ cells manufactured within this work is described by using the schematic cross sections depicted in Figure 1. These cross sections show the state of the cell symmetry element after every selected process step. Cells referred to as *initial type* feature one heat-treatment: the co-diffusion process (7). Cells referred to as *drive-in type* feature two heat-treatments: the co-diffusion (7) and the drive-in process (9).

The BC-BJ solar cells were manufactured from *n*-type Czochralski grown monocrystalline silicon wafers (Cz-Si) with a base resistivity ρ_{base} of 4 Ωcm. One wafer with an edge length of 12.5 cm features 16 BC-BJ solar cells. Silicon ablation during saw damage removal,

cleaning, and single-side texturing processes led to a final wafer thickness between 140 and 150 µm. After cleaning, a phosphorus-doped silicate glass (PSG) was deposited on the front side of the cell. This PSG-layer acts as a P-diffusion source for the diffusion of the FSF. To prevent any chemical reactions of PSG with the environment, an additional undoped silicate glass (SiO_x) was deposited on top of PSG (1). Afterwards, a stack consisting of PSG and SiO_x was deposited on the rear side as well (2). The PSG on the rear side acts as P-diffusion source for the diffusion of the BSF. Since the BSF requires higher doping-levels compared to the FSF, the doping concentration of the PSG layer on the rear side needs to be adapted [4, 5]. After deposition of the PSG-SiO_x stacks, the PSG-SiO_x stack on the rear side was patterned (3). The positive structure of the PSG-SiO_x stack defines the structure of the BSF-region. Finally, a boron-doped silicate glass was deposited on the rear side (4). The BSG-layer acts as a B-diffusion source for emitter diffusion. Since the PSG-SiO_x stack on the rear side acts as a diffusion barrier against boron, the negative structure of the PSG-SiO_x stack defines the structure of the emitter region. All the functional thin layers like PSG, BSG and SiO_x were deposited by means of plasma enhanced chemical vapor deposition (PECVD). After BSG-deposition, the co-diffusion step was carried out (5). The formation of FSF, BSF, and emitter takes place simultaneously. After co-diffusion, the silicate glasses were etched back (6). Aiming at the realization of deeply diffused areas, an additional heat-treatment, the drive-in process, was performed after etching (7).
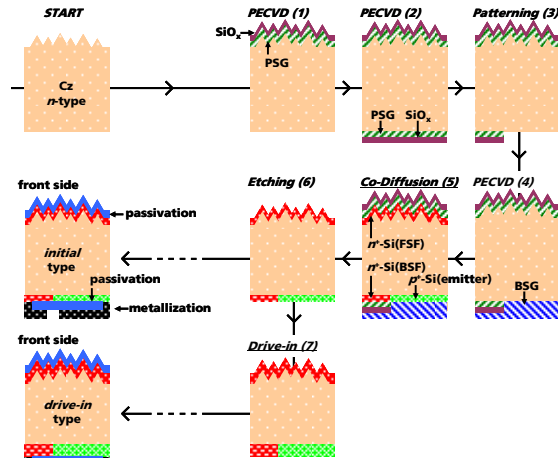

Figure 1: Process chain of the co-diffused BC-BJ cells. The initial type cell features only one heat-treatment. This is the co-diffusion process. The drive-in type cell features two heat-treatments. These are the co-diffusion and an additional drive-in process.

After the fabrication of the doping-structure, the front side of the cells was passivated by a PECVD-stack consisting of a silicon rich siliconoxynitride ($SiON_x$) film [6, 7] and a silicon nitride anti-reflection coating (AR-SiN_x). The cell rear side was passivated by a stack consisting of an atomic layer deposition (ALD) aluminum oxide (AlO_x) film [8, 9] and a PECVD-SiN_x film. Insulation layers for decoupling the metallization pattern from the doping pattern were not integrated yet [10]. To avoid spiking issues [11], the cells were metalized with an evaporated aluminum-silicon (Al-Si) alloy featuring a silicon content of 1 %. The contact

separation as well as all the other patterning steps were carried out wet chemically featuring a selectively inkjet-printed etching mask [12, 13]. The process chain was finished by an anneal, which is used for the saturation of dangling bonds and for the electrical contact formation.

2.2 Co-diffusion process

Within this work, phosphorus-doping and boron-doping is carried out with the help of phosphorus and boron-doped silicate glasses. The dopant content of these glasses and hence the dopant current density diffusing into silicon can be precisely adjusted by varying the process parameters of the corresponding PECVD-process [14-16].

For the deposition of BSG, the reactive gases diborane (B_2H_6), silane (SiH_4) and nitrous oxide (N_2O) are used. Since the deposition rate of BSG depends sensitively on the silane gas flow, the boron content within the BSG-layers depends on this parameter as well. Figure 2 shows the dependence of the emitter sheet resistance $R_{sh,p+}$ on the silane gas flow Q_{SiH4} as used during PECVD of BSG. For orientation, a schematic cross section of the BC-BJ cell during co-diffusion is depicted as well. The cross section (top) depicts the position of the PCVD-layers (BSG, PSG, SiO_x), the corresponding doped areas, and the area of interest for B-diffusion from BSG.
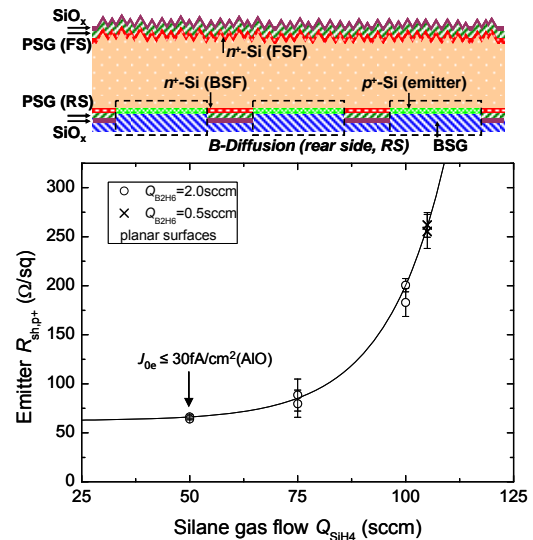

Figure 2: Dependence of the sheet resistance $R_{sh,p+}$ on the silane Q_{SiH4} and the diborane gas flow Q_{B2H6} during PECVD. The diffusion is carried out with a maximum temperature of 950°C and a plateau time of 30 minutes. Within the schematic cross section of the BC-BJ cell (top, co-diffusion state), the areas of B-diffusion are highlighted by dashed borders.

The sheet resistance increases with an increasing silane gas flow and is independent of the diborane gas flow in the investigated range. By varying the silane gas flow, a precise adjustment of the sheet resistance in the range of 60 to 300 Ω/sq is possible. BC-BJ adequate emitters have several requirements. On the one hand, high boron surface concentrations are necessary to enable low contact resistances between the metallization and silicon, on the other hand, deeply doped areas are advantageous since spiking issues can be avoided [17]. Low recombination currents are needed as well, since the

emitter coverage of efficient BC-BJ cells is high and hence has a strong impact on the open circuit voltage of the cell [18]. The usage of a BSG-layer deposited with a silane gas flow of 50 sccm results in a doped area with a low sheet resistance less than 70 Ω/sq. The dark emitter saturation current density (J_{0e}) of these doped areas is lower than 30 fA/cm^2 and, hence, all the above mentioned BC-BJ requirements can be fulfilled.

The phosphorus-content and hence the phosphorus-diffusion from PSG can be easily adjusted by varying the silane gas flow as well. For the deposition of PSG, diborane is replaced by trimethylphosphite (TMPi) as dopant precursor. The dependence of the sheet resistance $R_{sh,n+}$ on the silane gas flow Q_{SiH4} as used during PECVD of PSG is depicted in Figure 3.

The sheet resistance increases with an increasing silane gas flow as well and can be adjusted in a range of 30 Ω/sq to 400 Ω/sq. The FSF of a BC-BJ cell requires low recombination currents to provide high open circuit voltages and short circuit currents and a high lateral conductivity to decrease series resistance losses [19]. Doped areas diffused from PSG deposited with a silane gas flow of 60 sccm provide both, a sufficiently low sheet resistance and a low dark FSF saturation current density (J_{0FSF}) less than 60 fA/cm^2.
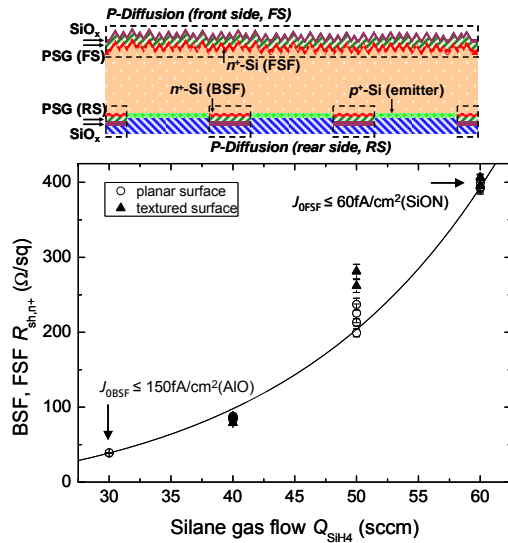

Figure 3: Dependence of the sheet resistance $R_{sh,n+}$ on the silane gas flow Q_{SiH4} during PECVD on planar and textured surfaces. The diffusion is carried out with a maximum temperature of 950°C and a plateau time of 30 minutes. Within the schematic cross section of the BC-BJ cell (top, co-diffusion state), the areas of P-diffusion are highlighted by dashed borders.

The BSF of a BC-BJ generally requires high phosphorus doping levels due to several reasons. Firstly, ohmic contacts between Al and n^+-Si featuring low electrical resistances are possible [17]. Secondly, field effect passivation can be exploited to decrease dark saturation current densities underneath interfaces with high surface recombination velocities like e.g. the metal contact [20]. Thirdly, the inversion influenced by the negatively charged Al$_2$O$_3$-layer and corresponding shunts can be avoided or rather limited [21].

Doped areas diffused from PSG deposited with a silane gas flow of 30 sccm provide a high doping-level with a sheet resistance less than 50 Ω/sq. These doped

areas feature a dark BSF saturation current density (J_{0BSF}) less than 150 fA/cm^2. The impact of the relatively high J_{0BSF} on the open circuit voltage of the BC-BJ cell an be limited by decreasing the area fraction of the BSF on the rear side.

2.2 Drive-in process

The so-called drive-in process has several advantages for the BC-BJ cell performance. Due to the additional heat-treatment without any diffusion sources, the doped areas get deeper and the dopant surface concentration decreases. On the one hand, this can lead lower dark saturation current densities, on the other hand, spiking issues might be further limited. In the following, the effect of the drive-in process on the concentration profile of the differently doped areas is explained. The measurements are carried out by electrochemical capacitance voltage (ECV) measurements.
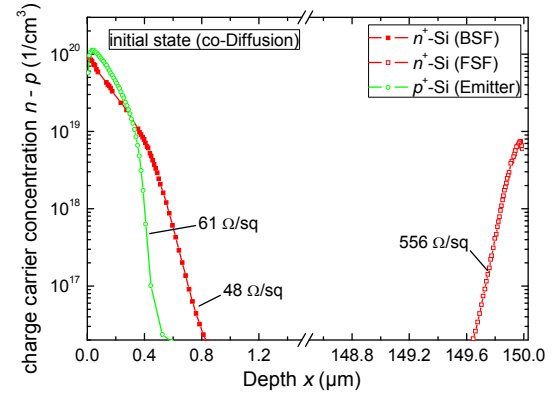

Figure 4: Concentration profiles of the BSF, FSF and the emitter in initial state (after co-Diffusion).
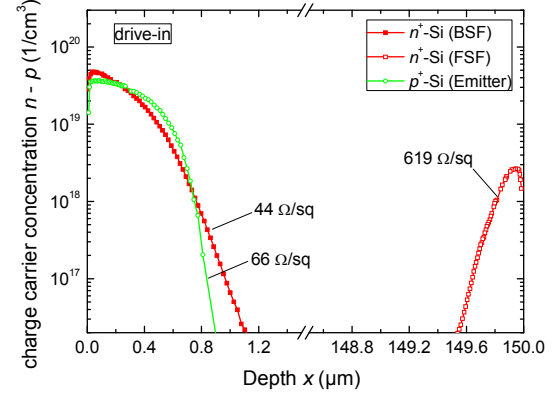

Figure 5: Concentration profiles of the BSF, FSF and the emitter after drive-in. Compared to the concentrations profiles in the upper graph, the charge carrier concentration decreases and the depth increases.

Figure 4 depicts the electron concentration $n(x)$ and $p(x)$ of the doped areas in the initial state (co-diffusion). Since no significant amount of inactive dopants is expected, the measured carrier concentration represents the dopant concentration. The emitter exhibits a maximum dopant concentration of $1 \cdot 10^{20}$ 1/cm^3. The pn-junction is located at a depth of approximately 600 nm. Since the FSF and the BSF are diffused from finite diffusion sources (thin PSG-layers), the phosphorus surface concentration of both is quite low leading to concentration profiles without the typical so-called kink-

and-tail shape. Suggesting ideal silicon surface conditions, the concentration profiles provide both, a high passivation ability leading to a low dark saturation current density as well as a high contacting ability of silicon by evaporated Al-Si alloys leading to a low specific contact resistivity.

Figure 5 shows the concentration profiles of the doped areas after the drive-in process. The influence of the drive-in process is clearly visible: for each profile the surface concentration decreases whereas the depth of the doped areas increases. Depending on the thermal budget during the drive-in process, the profiles can be adjusted to be even deeper.

3 SOLAR CELL RESULTS

3.1 Impact of the drive-in

Table I lists the cell parameters extracted from the *IV*-curve (one sun conditions). Shown is the mean value for each cell parameter and cell-type (4 cells measured per cell-type). The cell parameters of the best cell per cell-type are highlighted as well. Compared are cells featuring an initial doping structure (initial) and an additional drive-in step.

Table I: Cell parameters of comparable cells with and without drive-in. For the measurements, a busbar shading aperture with a designated area of 4 cm^2 was used.

Type ()	V_{OC} (mV)	J_{SC} (mA/cm^2)	FF (%)	pFF (%)	η (%)
Initial					
mean	632.7	38.1	73.4	77.5	17.7
best	639.3	38.7	74.3	77.9	18.4
Drive-in					
mean	653.0	40.4	73.8	79.7	19.5
best	653.3	40.5	75.7	80.1	20.0
calibrated	657.2	40.7	75.6		20.2

A strong increase in cell-efficiency is detectable for the cells with drive-in. To a great extent the increase in cell efficiency can be attributed to an increase in J_{SC} but also to a slight increase in V_{OC}. This improvement in cell performance is caused by the decreased dopant concentration within the doped areas leading to a lower surface recombination velocity especially on the front side. The pseudo fill factor pFF (SunsVOC, [22]) indicates a less pronounced cell shunting due to Al-spiking as well as a lower recombination in the space charge region. Since the space charge region is wider for decreased dopant concentrations as realized by the cells with drive-in, less shunting due to tunneling currents can be expected.

3.2 Impact of the BSG deposition process

The cells manufactured within this work were fabricated with two different BSG-deposition processes. The setups of the two depositions processes are completely different. In the following executions the deposition processes are differentiated according to the plasma activation. The first process uses microwaves for plasma activation (MW-BSG). A linear antenna is used for coupling in microwaves in the process chamber. The second process uses a so-called capacitor configuration. The energy for plasma activation is coupled in electrically with an alternating voltage ($f = 13.56$ MHz,

radio frequency *rf*). This process is called the *rf*-BSG process. The cell parameters of the cells are depicted in Table II.

A strong increase in cell efficiency is detectable for cells being manufactured with the *rf*-BSG deposition process. As already mentioned, this process uses an *rf*-source instead of a MW-source for plasma activation as well as shorter deposition times. The corresponding cells feature an increase in V_{OC}, J_{SC}, and FF resulting in an absolute efficiency gain $\Delta_{abs}\eta$ of 1.5 %. The increased V_{OC} as well as J_{SC} are probably due to a higher bulk life time. The increased pFF might be attributed to fewer impurities in the space charge region.

In general, the cells feature special characteristics: A high J_{SC} values and a low FF. In the following chapter a modification of the metallization is carried out, aiming at an increase in FF.

Table II: Cell parameters of comparable cells manufactured with two different BSG-deposition processes. For the measurements, a busbar shading aperture with a designated area of 4 cm^2 was used.

Type ()	V_{OC} (mV)	J_{SC} (mA/cm^2)	FF (%)	pFF (%)	η (%)
MW-BSG					
mean	638.0	38.4	71.4	76.9	17.5
best	642.4	38.5	73.0	78.6	18.1
rf-BSG					
mean	646.5	39.6	74.3	79.5	19.0
best	650.0	40.1	74.3	79.9	19.4
calibrated	654.0	40.3	74.3		19.6

4 SOLAR CELL IMPROVEMENT

As already discovered within the *IV*-measurements, a high difference between pFF and FF is present for every cell. This difference between pFF and FF is related to series resistance losses. Hence, also the cells presented within this work probably suffer from series resistance losses. Besides intrinsic series resistance losses in silicon, also the extrinsic losses due to a non ideal metallization might be crucial. These extrinsic losses might be caused by a high contact resistance between metallization and silicon, but also by a high resistance of the interdigitated grid.

Table III: Cell parameters of the best cells with and without drive-in after plating. For the measurements, a busbar shading aperture with a designated area of 4 cm^2 was used.

Type ()	V_{OC} (mV)	J_{SC} (mA/cm^2)	FF (%)	pFF (%)	η (%)
Drive-in, MW-BSG					
	656.1	40.6	74.9	80.8	19.9
plating	655.8	40.7	75.9	80.6	20.3
calibrated	658.7	40.9	76.0		20.5
Initial, rf-BSG					
	647.7	39.9	72.9	79.8	18.8
plating	652.0	40.2	74.5	79.9	19.5

Aiming at decreasing the resistance of the interdigitated grid, the Al-Si metallization was thickened by a plating process. Therefore, the surface of the Al-Si

metallization was modified by a zincate solution and afterwards thickened by Ag-plating [23].

Table III depicts the cell results of the best cells after plating. One cell features a drive-in process and an emitter diffused from the MW-source. The other cell dispenses with a drive-in process and integrates an emitter diffused from the *rf*-source. In both cases the *FF* increases after plating. This is due to the enlarged cross section of the metal fingers after plating. Simultaneously the p*FF* is almost constant before and after plating. Therefore, additional shunting problems can be neglected. For the cell featuring a drive-in, the increased *FF* induces an increase in cell efficiency up to 20.5 %. This efficiency is independently confirmed by the Fraunhofer ISE calibration laboratory (CalLab) and the highest efficiency value reached within this work so far. The best cell without drive-in process features a cell efficiency of 19.5 % after plating.

5 CONCLUSIONS AND OUTLOOK

Within this work BC-BJ solar cells are fabricated using Cz-Material. The process chain integrated a co-diffusion process, allowing for the diffusion of all the required doped areas in only one high temperature step. Therefore prepatterned doped silicate glasses are used. The best cells fabricated with only one heat-treatment step reach an efficiency of 19.7 %. By implementing a second heat-treatment, the drive-in process, this efficiency can be further increased to 20.5 %. The best cell features high short circuit current densities up to 40.9 mA/cm^2 on the one hand, and yet, moderate fill factors and open circuit voltages, on the other hand. Especially the *FF* indicates the high potential of this very promising cell-type. Further studies will focus on the improvement of the fill factor and the open circuit voltage. The integration of defect free insulation layers on the cell rear side, design studies, as well as up scaling the cell format are key issues for future investigation.

6 ACKNOWLEDGEMENT

7 REFERENCES

[1]   P. J. Cousins, D. D. Smith, H.-C. Luan, J. Manning, T. D. Dennis, A. Waldhauer, K. E. Wilson, G. Harley, and W. P. Mulligan, "Generation 3: improved performance at lower cost," presented at Proceedings of the 35th IEEE Photovoltaic Specialists Conference, Honolulu, Hawaii USA, 2010.

[2]   K. Nakamura, M. Kohira, Y. Abiko, T. Isaka, Y. Funakoshi, and T. Machida, "Development of back contact si solar cell and module in pilot production line," presented at Proceedings of the 23rd European Photovoltaic Solar Energy Conference, Valencia, Spain, 2008.

[3]   R. Keding, D. Stüwe, M. Kamp, C. Reichel, A. Wolf, R. Woehl, D. Borchert, H. Reinecke, and D. Biro, "Co-diffused back-contact back-junction silicon solar cells without gap regions," *IEEE Journal of Photovoltaics*, vol. 3, issue 4, pp. 1-7, 2013.

[4]   A. G. Aberle, S. Glunz, and W. Warta, "Field effect passivation of high efficiency silicon solar cells," *Solar Energy Materials and Solar Cells*, vol. 29, pp. 175-82, 1993.

[5]   D. K. Schroder and D. L. Meier, "Solar cell contact resistance - a review," *IEEE Transactions on Electron Devices*, vol. ED-31, pp. 637-47, 1984.

[6]   J. Seiffe, L. Weiss, M. Hofmann, L. Gautero, and J. Rentsch, "Alternative rear surface passivation for industrial cell production," presented at Proceedings of the 23rd European Photovoltaic Solar Energy Conference, Valencia, Spain, 2008.

[7]   C. Schwab, M. Hofmann, J. Rentsch, and R. Preu, "Front surface passivation for industrial-type solar cells by silicon oxynitride - silicon nitride stacks," *Proceedings of the 25th European Photovoltaic Solar Energy Conference and Exhibition*, pp. 2307-10, 2010.

[8]   B. Hoex, J. Schmidt, P. Pohl, M. C. M. van de Sanden, and W. M. M. Kessels, "Silicon surface passivation by atomic layer deposited Al$_2$O$_3$," *Journal of Applied Physics*, vol. 104, pp. 044903, 2008.

[9]   A. Richter, J. Benick, M. Hermle, and S. W. Glunz "Excellent silicon surface passivation with 5 Å thin ALD Al$_2$O$_3$ layers: influence of different thermal post-deposition treatments," *Physica Status Solidi RRL*, vol. 5-6, pp. 202-4, 2011.

[10]   C. Reichel, M. Reusch, F. Granek, M. Hermle, and S. W. Glunz, "Decoupling charge carrier collection and metallization geometry of back-contacted back-junction silicon solar cells by using insulating thin films," presented at Proceedings of the 35th IEEE Photovoltaic Specialists Conference, Honolulu, Hawaii, USA, 2010.

[11]   M. Manole, R. Meyer, P. Engelhart, and R. Brendel, "Effective methods to increase thermal stability of shallow emitter solar cells with aluminium front contacts," presented at Proceedings of the 20th European Photovoltaic Solar Energy Conference, Barcelona, Spain, 2005.

[12]   J. Specht, D. Biro, N. Mingirulli, M. Aleman, U. Belledin, R. Efinger, D. Erath, L. Gautero, A. Lemke, D. Stüwe, J. Rentsch, and R. Preu, "Using hotmelt-inkjet as a structuring method for higher efficiency industrial silicon solar cells," presented at Proceedings of the International Conference on Digital Printing Technologies and Digital Fabrication, Pittsburgh, PA, USA, 2008.

[13]   N. Mingirulli, R. Keding, J. Specht, A. Fallisch, D. Stüwe, and D. Biro, "Hot-melt inkjet as masking technology for back-contacted cells," presented at Proceedings of the 34th IEEE Photovoltaic Specialists Conference, Philadelphia, 2009.

[14]   A. Fallisch, D. Wagenmann, R. Keding, D. Trogus, M. Hofmann, J. Rentsch, H. Reinecke,

and D. Biro, "Analysis of phosphorus-doped silicon oxide layers deposited by means of PECVD as a dopant source in diffusion processes," *IEEE Journal of Photovoltaics*, vol. 2, pp. 450-6, 2012.

[15] R. Keding, R. Woehl, D. Stüwe, A. Fallisch, A. Hofmann, J. Rentsch, and D. Biro, "Diffusion and characterization of doped patterns in silicon from prepatterned boron- and phosphorus-doped silicate glasses," presented at Proceedings of the 26th European Photovoltaic Solar Energy Conference and Exhibition, Hamburg, Germany, 2011.

[16] B. Bazer-Bachi, C. Oliver, B. Semmache, Y. Pellegrin, M. Gauthier, N. Le Quang, and M. Lemiti, "Co-diffusion from boron doped oxide and POCl$_3$," presented at Proceedings of the 26th European Photovoltaic Solar Energy Conference and Exhibition, Hamburg, Germany, 2011.

[17] D. K. Schroder and D. L. Meier, "Solar-Cell Contact Resistance - a Review," *Ieee Transactions on Electron Devices*, vol. 31, pp. 637-647, 1984.

[18] S. Kluska, F. Granek, M. Rüdiger, M. Hermle, and S. W. Glunz "Modeling and optimization study of industrial n-type high-efficiency back-contact back-junction silicon solar cells," *Solar Energy Materials and Solar Cells*, vol. 94, pp. 568-77, 2010.

[19] F. Granek, C. Reichel, M. Hermle, D. M. Huljic, O. Schultz, and S. W. Glunz, "Front surface passivation of n-type high-efficiency back-junction silicon solar cells using front surface field," presented at Proceedings of th 22nd European Photovoltaic Solar Energy Conference Milan, Italy, 2007.

[20] A. G. Aberle, W. Warta, J. Knobloch, and B. Voß, "Surface passivation of high-efficiency silicon solar cells," presented at Proceedings of the 21st IEEE Photovoltaic Specialists Conference, Kissimmee, Florida, USA, 1990.

[21] S. Dauwe, L. Mittelstädt, A. Metz, and R. Hezel, "Experimental evidence of parasitic shunting in silicon nitride rear surface passivated solar cells," *Progress in Photovoltaics: Research and Applications*, vol. 10, pp. 271-8, 2002.

[22] R. A. Sinton and A. Cuevas, "A quasi-steady-state open-circuit voltage method for solar cell characterization," presented at Proceedings of the 16th European Photovoltaic Solar Energy Conference, Glasgow, UK, 2000.

[23] M. Kamp, J. Bartsch, G. Cimiotti, R. Keding, A. Zogaj, C. Reichel, A. Kalio, M. Glatthaar and S. W. Glunz, "Zincate processes for silicon solar cell metallization,"
Solar Energy Materials & Solar Cells, 2013, http://dx.doi.org/10.1016/j.solmat.2013.05.035i
.